

Assessment of the early organization and maturation of infants' cerebral white matter fiber bundles: A feasibility study using quantitative diffusion tensor imaging and tractography

J. Dubois,^{a,b,*} L. Hertz-Pannier,^{a,b,c,d} G. Dehaene-Lambertz,^{a,b,e}
Y. Cointepas,^{a,b} and D. Le Bihan^{a,b}

^aCEA, Service Hospitalier Frédéric Joliot, Orsay, F91401, France

^bIFR49, Paris, France

^cAP-HP, Hôpital Necker-Enfants Malades, Radiologie Pédiatrique, Paris, F75015, France

^dINSERM, U663, Paris, F75015, France

^eINSERM, U562, Orsay, F91401, France

Received 4 April 2005; revised 28 October 2005; accepted 4 November 2005
Available online 18 January 2006

The human infant is particularly immature at birth and brain maturation, with the myelination of white matter fibers, is protracted until adulthood. Diffusion tensor imaging offers the possibility to describe non invasively the fascicles spatial organization at an early stage and to follow the cerebral maturation with quantitative parameters that might be correlated with behavioral development. Here, we assessed the feasibility to study the organization and maturation of major white matter bundles in eighteen 1- to 4-month-old healthy infants, using a specific acquisition protocol customized to the immature brain (with 15 orientations of the diffusion gradients and a $700 \text{ s mm}^{-2} b$ factor). We were able to track most of the main fascicles described at later ages despite the low anisotropy of the infant white matter, using the FACT algorithm. This mapping allows us to propose a new method of quantification based on reconstructed tracts, split between specific regions, which should be more sensitive to specific changes in a bundle than the conventional approach, based on regions-of-interest. We observed variations in fractional anisotropy and mean diffusivity over the considered developmental period in most bundles (corpus callosum, cerebellar peduncles, cortico-spinal tract, spinothalamic tract, capsules, radiations, longitudinal and uncinate fascicles, cingulum). The results are in good agreement with the known stages of white matter maturation and myelination, and the proposed approach might provide important insights on brain development.

© 2005 Elsevier Inc. All rights reserved.

Keywords: Brain; Development; Infant; Myelination; Diffusion tensor imaging; Tractography

Introduction

Brain white matter myelination is a long process which starts well before birth and continues until adulthood. Post-mortem studies have shown that myelination progresses in a caudo-rostral way, at different rates depending on location (Yakovlev and Lecours, 1967; Brody et al., 1987), with earlier maturation of motor and sensory tracts in comparison with cortico-cortical association fibers. This long-lasting process has been confirmed in vivo with conventional Magnetic Resonance Imaging (MRI) (Barkovich et al., 1988; Van der Knaap and Valk, 1990; for review Paus et al., 2001), which provides images of the infant brain in three dimensions (3D) and non invasively. Recently, Diffusion Weighted Imaging (DWI) and Diffusion Tensor Imaging (DTI) have proved to be more sensitive to explore brain development and white matter fibers density and maturation (Rutherford et al., 1991; Sakuma et al., 1991; for review Neil et al., 2002), since the early bundles organization can be depicted and the monitored parameters are changing in the immature brain earlier than the T1 and T2 relaxation times (Huppi et al., 1998a; Neil et al., 1998; Baratti et al., 1999).

Diffusion MRI permits biological tissue structure to be probed and imaged on a microscopic scale non invasively (Le Bihan et al., 1986; for review Le Bihan, 2003). Because water diffuses more easily in the direction of the fibers than orthogonally, where it is hindered by myelin sheaths or axonal membranes, this technique has been used to study the organization of the adult white matter in fiber bundles (Moseley et al., 1990). In order to get information on the diffusion “anisotropy”, images are acquired in DTI with several diffusion-encoding gradients, applied in non collinear orientations (Basser et al., 1994; for reviews Le Bihan et al., 2001; Basser and Jones, 2002). With post-processing algorithms, 3D “tracking” of brain connections becomes possible (Conturo et

* Corresponding author. SHFJ / CEA, 4 place du General Leclerc, 91 401 Orsay cedex, France. Fax: +33 1 69 86 77 86.

E-mail address: jdubois@shfj.cea.fr (J. Dubois).

Available online on ScienceDirect (www.sciencedirect.com).

al., 1999; Mori et al., 1999; for review Mori and van Zijl, 2002) and enables an in vivo “dissection” of several main fascicles (Catani et al., 2002, 2003; Mori et al., 2002; Hagmann et al., 2003) and the construction of atlases of white matter bundles (Wakana et al., 2004). But, so far, all these bundles have only been mapped in adults’ fully myelinated brains.

Yet, large degree of anisotropy is already present in non-myelinated nerves (Beaulieu and Allen, 1994), as well as in the white matter of premature newborns (Huppi et al., 1998a) and of young animals (Wimberger et al., 1995; Prayer et al., 2001), with not or poorly myelinated fibers. These observations point out that bundles are spatially organized early on and should be accessible to imaging. Indeed, major commissural, projection and association fascicles have been identified in two dimensions (2D) in the neonatal brain, preterm or at term (Partridge et al., 2004; Hermoye et al., *in press*), and recently tracked in 3D (corpus callosum: Zhai et al., 2003; some projection tracts: Yoo et al., 2005). Nevertheless, the whole structure of white matter bundles has not been reconstructed in infants with tractography like in adults.

Besides the visualization of white matter tracts, DTI should also provide an evaluation of the bundle maturation, since the diffusion parameters (mean diffusivity, indexes of anisotropy) vary with the water content and the fibers’ compactness and myelination. Changes with age have been described in newborns (Neil et al., 1998; Huppi et al., 1998a) and infants from birth to childhood (Mukherjee et al., 2001). Because the first months of life represent a critical period, during which the cerebral growth is intense (the cranial perimeter increases of 0.5 cm per week) and the brain encounters various and numerous stimulations (after a “protected” period during gestation), we need a more precise description of the differential maturation across bundles at this time period. Such a study requires a reliable and reproducible method of volumes-of-interest (VOIs) definition for the diffusion parameters quantification, in order to allow subtle changes to be detected. Hence, the conventional approach, based on regions-of-interest (ROIs), may not be appropriate because of intrinsic difficulties (location variability across subjects, partial volume effects), whereas performing measurements directly on the tracked bundles seems more accurate.

In this context, DTI and fiber tracking were used to assess the early 3D organization and maturation of white matter bundles in eighteen 1- to 4-month-old unsedated healthy infants. A specific acquisition protocol was designed to study the immature infant’s brain with appropriate spatial resolution, while dealing with motion artifact issues. Several incompletely myelinated fascicles were mapped in 3D using fiber tracking, and the tracts were compared to the adult bundles for identification. An original method for quantifying diffusion parameters in bundles, based on tracking, was developed and compared to the conventional approach by ROIs. Changes in mean diffusivity and fractional anisotropy were then monitored over the considered developmental period.

Materials and methods

Subjects

Twenty-five healthy infants were included in this study after their parents gave written informed consent. Reliable data were obtained only for eighteen infants (mean chronological age: 12.9 ± 3.4 weeks, range: 6.6–19.4 w; mean maturational age, i.e.

corrected by gestational age at birth: 11.2 ± 3.6 weeks, range: 5.4–18.4 w) because no sedation was used. These infants were spontaneously asleep during MR imaging. The infant gestational age at birth was known with an uncertainty smaller than 3 days as the first US examination was performed before 12 weeks of gestation. Particular precautions were taken to minimize the noise exposure, by using customized headphones and by covering the magnet tunnel with a special noise protection foam. The study was approved by a regional ethical committee for biomedical research.

Data acquisition

The acquisition was performed on a 1.5-T MRI system (Signa LX, GEMS, USA), with a maximum gradient amplitude of 22 mT m^{-1} and using a birdcage head coil. A diffusion-weighted (DW) spin-echo echo-planar technique was implemented, with a 700 s mm^{-2} b factor (TE/TR = 89.6 ms/13.8 s) and 15 diffusion gradient encoding orientations. A specific orientation scheme was designed to avoid losing the whole data set in case of motion during acquisition (Dubois et al., 2004). Thirty interleaved axial slices covering the whole brain were acquired (slice thickness = 2.5 mm, FOV = 24 cm, matrix = 128×128); the in-plane resolution was interpolated to $0.94 \times 0.94 \text{ mm}^2$ at reconstruction. The acquisition time was of 3 min 40 s.

Efforts were made to obtain a reproducible signal-to-noise ratio (SNR) among infants brains. Additional orientations were thus acquired in nine infants in order to improve SNR. In three other infants, images of one orientation were removed before post-processing, because of cortico-spinal fluid (CSF) pulsatility artifacts or motion. Hence, the orientations count varied slightly across infants.

Finally, conventional anatomical MR images were acquired using a fast spin-echo sequence, yielding a T2 weighting for the best contrast between grey and white matter, in order to provide a precise anatomical reference.

Data post-processing

Data processing was performed using Anatomist (Riviere et al., 2000, <http://anatomist.info>) and BrainVISA softwares (Cointepas et al., 2001, 2003, <http://brainvisa.info/>).

Image preparation

The geometric distortions of the DW images, due to eddy currents, were corrected referring to the $b = 0$ image (Mangin et al., 2002). No correction of motion artefacts was performed in the DW images. The DW and anatomical images were then co-registered. After the anterior and posterior commissures (AC and PC) were labeled on the anatomical images, all images were realigned in the AC–PC plane and diffusion orientations were reoriented.

Diffusion tensor estimation

The diffusion tensor was estimated on a pixel-by-pixel basis and diagonalized. Mean diffusivity ($\langle D \rangle$) and fractional anisotropy (FA) were calculated (Basser and Pierpaoli, 1996; Pierpaoli and Basser, 1996). This anisotropy index ranges between 0 for an isotropic tissue and 1 for a perfectly anisotropic tissue. A map of color-coded directionality (RGB map) was generated, in which the color codes for the principal eigenvector orientation (red: right–left; green: anterior–posterior; blue: inferior–superior), while the contrast is weighted with FA (Pajevic and Pierpaoli, 1999).

Detection of the white matter fiber bundles

2D identification

First, the following fiber bundles were identified on the RGB map (see Results, Fig. 2), using anatomical atlases obtained in infants with conventional MRI (Salamon et al., 1990) and in adults with DTI (Wakana et al., 2004), as well as post-mortem dissections:

- Commissural fibers: corpus callosum (1) genu (1a), splenium (1b), body (1c), middle cerebellar peduncles (2), pontine crossing tract (3).
- Projection fibers: spino-thalamic tract and medial lemniscus (4), cortico-spinal fibers (5) (in the mid-brain (6), cerebral peduncles (7), posterior limb of the internal capsule (8), low (9) and high (10) centrum semiovale), anterior limb of the internal capsule (11), optic (12) and acoustic (13) radiations.
- Association fibers: external capsule (14), superior (15) and inferior (16) longitudinal fascicles, uncinate (17) fasciculus, cingulum (18). The inferior fronto-occipital fasciculus was not identified because it merges with the uncinate fasciculus in the frontal region and in the inferior part of the external/extreme capsule and with the inferior longitudinal fasciculus in the occipital region.

Fiber bundles tractography

Second, the identified fiber bundles were reconstructed in 3D using the linear FACT algorithm (“Fiber Assignment by Continuous Tracking”, Mori et al., 1999). The “tracking” was performed on a voxel-by-voxel basis by continuously following the orientation of the tensor first eigenvector. All fiber bundles passing through a “seed” positioned on the bundle were tracked, with some constraints dependant on the bundles. A FA threshold of 0.1 was used. The “curvature angle” (angle between the first eigenvector and the tract tangential vector) was imposed to be smaller than 60° for the uncinate fasciculus (which has the most curved geometry) and 45° for the other bundles.

The reliability of the obtained bundles was evaluated according to a priori knowledge on the adult bundles organization. The fibers were selected and classified according to the regions they run across, so that artefactual fibers were avoided (“two regions-of-interest” approach described in Catani et al., 2002); two to four “selection regions” were used (see Results, Fig. 4 and Table 1 for the regions count). The corpus callosum genu and splenium were defined as the connection pathways between the frontal lobes, and the occipital and parietal lobes, respectively; the other fibers of the corpus callosum were supposed to belong to the corpus callosum body. The pyramidal tract was defined as the fibers passing through the cerebral peduncles, the posterior limb of the internal capsule and the low and high centrum semiovale. The anterior limb of the internal capsule traveled between the genu of the internal capsule and the frontal lobe. Fibers of the external capsule ran in an inferior–superior direction, through the capsule and the low centrum semiovale. Optic radiations connected the lateral geniculate nucleus and the occipital pole, whereas the inferior longitudinal fasciculus connected the temporal and occipital lobes. Finally, the uncinate fasciculus connected the frontal and the temporal lobes, and passed through the inferior part of the external/extreme capsule.

Table 1

Tracking results across infants (cereb ped: cereblar peduncles; ic: internal capsule; lcs: low centrum semiovale; hcs: high centrum semiovale)

Bundle	Regions count	Tracts /18		Infants/18
		L	R	
Corpus callosum:				
Genu	1a	2		18
Splenium	1b	2		18
Body	1c	2		18
Spino-thalamic tract	4	2	18	18
Cortico-spinal tract:				
Midbrain-hcs		5	12	9
Cereb ped-hcs	5	4	18	18
Midbrain-cereb ped	6	2	18	13
Cereb ped-ic	7	2	18	18
ic-lcs	8	2	18	18
Lcs-hcs	9	2	18	18
ic anterior limb	11	2	18	18
Optic radiations	12	2	15	14
External capsule	14	2	18	18
Inferior longitudinal:	16	3	10	12
In the temporal region	16a	2	16	16
In the occipital region	16b	2	18	17
Uncinate:	17	3	11	11
In the frontal region	17a	2	16	13
In the temporal region	17b	2	18	17
“All”	19	–	12	10

Are outlined the count of “selection regions” used for each bundle, the number of reliable tracts (over 18) obtained in left (L) and right (R) hemispheres and the number of infants for which the bundles were tracked at least on one side.

Diffusion parameters quantification in white matter bundles

Definition of regions and tracts of interest

In order to assess the maturation degree of the white matter fascicles, FA and $\langle D \rangle$ were measured in the previously described individual bundles, averaged over both manually drawn ROIs and sections of the tracked bundles. The ROIs’ and tracking seeds’ localization was performed concomitantly for all infants to increase the reliability. The ROIs and tracts were labeled with a “r” and “t” prefixed to the bundle numbers, respectively (“rN”/“tN” for the Nth bundle).

First, polygonal ROIs were positioned in each identified bundle, in both hemispheres, using both the $b = 0$ image and the RGB map (see results Fig. 2 for a survey of the ROIs location). The region’s volume depended on the bundle (between 65 mm³ and 130 mm³), and it was sufficiently small so that the whole ROI was located in the bundle core. For the inferior longitudinal fasciculus, two ROIs were identified, in the temporal (r16a) and occipital (r16b) lobes. For the uncinate fasciculus, three ROIs were drawn, in the frontal region (r17a), in the inferior part of the external/extreme capsule (r17b) and in the temporal lobe (r17c).

Second, the analysis was performed in sections of the reconstructed tracts. The fibers were split at the level of specific regions (see results Fig. 4 for a survey of the splits location), and we checked that the tract sections did not run within gray matter using the $b = 0$ image. The corpus callosum genu (t1a) and splenium (t1b) were sectioned at 9.4 mm from the inter-hemispheric scissure on both sides, so that they did not merge with the forceps minor and major. The fibers of the corpus callosum body (t1c) were more limited and were sectioned at 4.7 mm from the scissure. The

cortico-spinal tract was divided into four sections (t6: 6–7, t7: 7–8, t8: 8–9, t9: 9–10). The spino-thalamic tract (t4) was constrained to the midbrain. The anterior limb of the internal capsule (t11) was sectioned between the capsule genu and the frontal region. Part of the external capsule (t12) was considered, between the “capsules level” and the low centrum semiovale. Two segments for the inferior longitudinal and the uncinate fascicles were considered, in the temporal (t16a) and occipital (t16b) regions, and in the frontal (t17a) and temporal (t17b) regions, respectively. For index quantification over a tract section, line integration for each fiber was used by interpolating $\langle D \rangle$ and FA maps in 3D: a mean value was calculated by averaging the measurements from all the points of all the bundle fibers.

Diffusion parameter averages between right and left hemispheres were considered, except when a bundle was not tracked on one side. When several ROIs or sections were identified at different locations of one fasciculus, mean FA and $\langle D \rangle$ were calculated over these ROIs or sections to characterize the bundle as a whole (corpus callosum: r1/t1: mean over 1a–c; cortico-spinal tract: r5/t5: mean over 6–10; inferior longitudinal fasciculus: r16/t16: mean over 16a–b; uncinate fasciculus: r18/t18: mean over 18a–c). Finally, the FA and $\langle D \rangle$ averages over all ROIs (r19) and over all tracts (t19) were calculated to evaluate the global maturation of the infants’ bundles.

Fiber bundles maturation: evolution of diffusion parameters with age

FA and $\langle D \rangle$ changes with age, corrected by gestational age at birth, were evaluated for each bundle and each method, using a linear regression. Statistically significant correlations were considered at a level of $P < 0.05$ (thresholds were corrected for multiple comparisons, with “false discovery rate” (FDR) approach), and the parameter variations were computed on a week by week basis.

Quantification methods: ROIs vs. tracts

The averages and standard deviations over infants of the diffusion parameters were recorded for the ROI and split tract

analyses. If a significant correlation with age were to be found in a bundle, the effect of age was removed prior to the standard deviation calculation. The methods were compared by testing the differences between the indexes (X_{ROI} vs. X_{tracts} , $X = FA$ or $\langle D \rangle$) using a two-tailed paired t test over infants (statistical threshold $P < 0.05$ after FDR correction). Finally, the results obtained for the changes with age were compared for both methods.

Results

White matter organization in fiber bundles

2D identification

The “effective SNR” of the $b = 0$ image (corrected for the acquired orientation count, in comparison with the reference of 15 orientations: $SNR_{effective} = SNR \cdot \sqrt{N_{orientations}/15}$) was of 31.9 ± 3.3 in white matter (mean \pm standard deviation over infants). High-quality diffusion tensor images were obtained with the proposed protocol (Fig. 1). Major bundles were identified in 2D, as outlined on the RGB map in Fig. 2. The spino-thalamic tract, the superior longitudinal and the uncinate fascicles were clearly visible, although they had not been previously described in infants.

Fiber bundles tractography

Fiber tracking was obtained for a part or the totality of all bundles (Fig. 3), except the pontine crossing tract and the cingulum. The tracking of the middle cerebellar peduncles was truncated in some infants, because the mid-brain was not imaged entirely. As described in adults, the tracking accuracy might be questionable with some bundles, especially in the places of crossing fibers, such as the acoustic radiations when they get close to the optic radiations or the optic radiations when they get close to the inferior longitudinal fasciculus.

In the absence of a reference for the white matter organization in infants, the tracking accuracy and reproducibility were increased

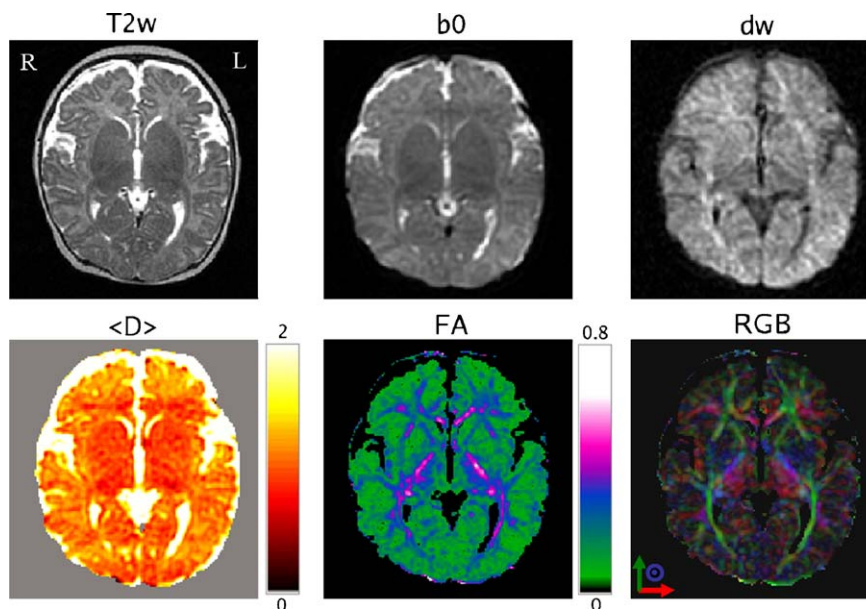


Fig. 1. DTI maps: anatomical (T2w), non-diffusion weighted (b_0) and diffusion weighted images (DW) and maps of $\langle D \rangle$ (scale: $10^{-3} \text{ mm}^2 \text{ s}^{-1}$), FA and RGB obtained on a 15.7-week-old infant (age corrected by gestational age at birth), at the level of the optic radiations. FA and RGB maps were masked for $\langle D \rangle$ values higher than $2 \times 10^{-3} \text{ mm}^2 \text{ s}^{-1}$. Images are presented with radiological convention: left (L) and right (R) are reversed.

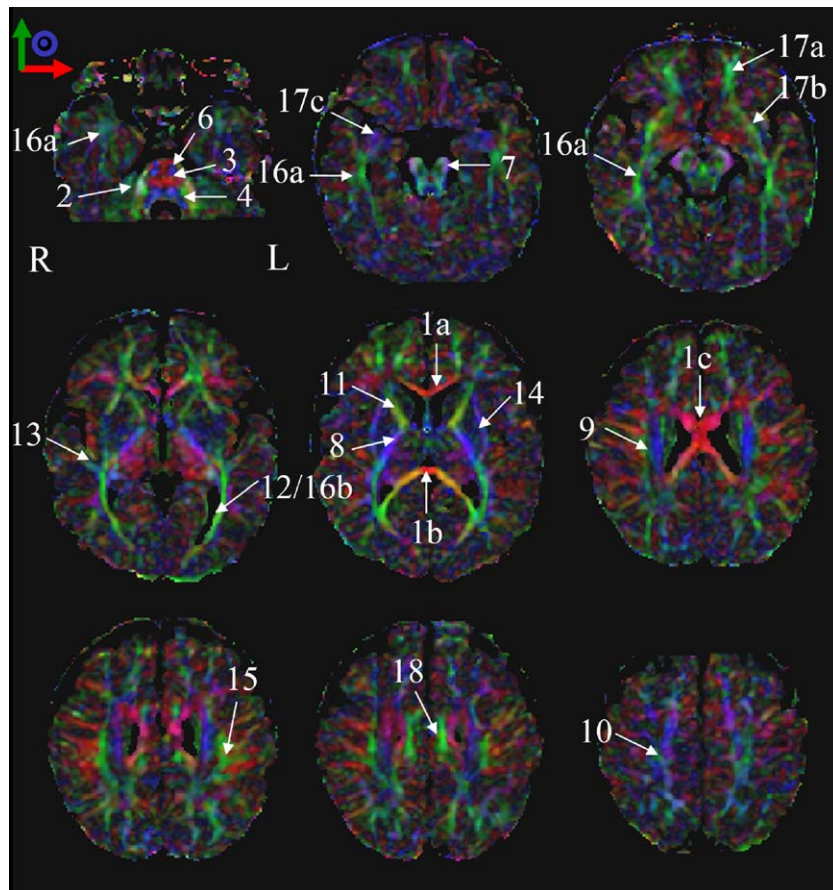


Fig. 2. Bundles identification: RGB maps obtained for the same infant, showing the identified bundles (see the text for the number significance). The bottom and top images are cut because the imaged volume was realigned in the AC–PC plane.

across infants by constraining the tracts to run through specific regions, given a priori knowledge on the bundles organization in adults (Figs. 4a–b). However, this approach was not used for some bundles: the cerebellar peduncles tracts were truncated in some infants, and the location of the acoustic radiations and the superior longitudinal fascicles was highly variable across infants. The results across infants are detailed in Table 1. For the pyramidal tract (5), partial volume effects in the midbrain did not provide fibers continuity from this region to the high centrum semiovale for six infants; the tract was thus defined as the fibers connecting the cerebral peduncles and the high centrum semiovale. For the inferior longitudinal and the uncinate fascicles, no fibers were found to continuously connect the three “selection regions” for six and three infants, respectively, and the two segments were thus considered individually.

Diffusion parameters quantification in white matter bundles

Volumes of interest

The location of the ROIs and tracts sections are outlined in Figs. 2 and 4c, respectively. The tract approach was not used for the middle cerebellar peduncles, the pontine crossing tract, the acoustic radiations, the superior longitudinal fasciculus and the cingulum because these bundles were not tracked or not reproducibly split over infants. Because the spatial resolution remained coarse compared to the infant bundles size, the uniformity of the diffusion parameters, particularly FA, was quite

low within the VOIs for both the ROI and tract approaches. However, the intra-regional variabilities were deeply reproducible across infants, and the mean parameters, averaged over the VOIs, were computed as indexes characterizing the bundles regions.

Fiber bundles maturation: evolution of diffusion parameters with age

Statistically significant correlations of diffusion parameters with age, corrected by gestational age at birth, were obtained for most bundles with both methods (Table 2, Fig. 5). Both FA and $\langle D \rangle$ changed with age in the corpus callosum splenium and body, the pontine crossing tract, the cortico-spinal tract below the low centrum semiovale, the capsules, the optic and acoustic radiations, the superior and inferior (on average, region 16) longitudinal fascicles, the cingulum and the global white matter; in the optic radiations and the inferior longitudinal fasciculus, the FA increase was observed with the tract approach only. Isolated $\langle D \rangle$ decreases (not related to FA increases) were found in the centrum semiovale, the segments of the inferior longitudinal bundle, the uncinate fasciculus, and, with the ROI approach, in the corpus callosum genu and the middle cerebellar peduncles. Isolated FA increases (not related to $\langle D \rangle$ decreases) were observed in the spino-thalamic tract with the tract approach. The variations in the diffusion parameters with age were well beyond experimental error, as the changes, reported to the age period of 13 weeks, were larger than the standard deviations over infants.

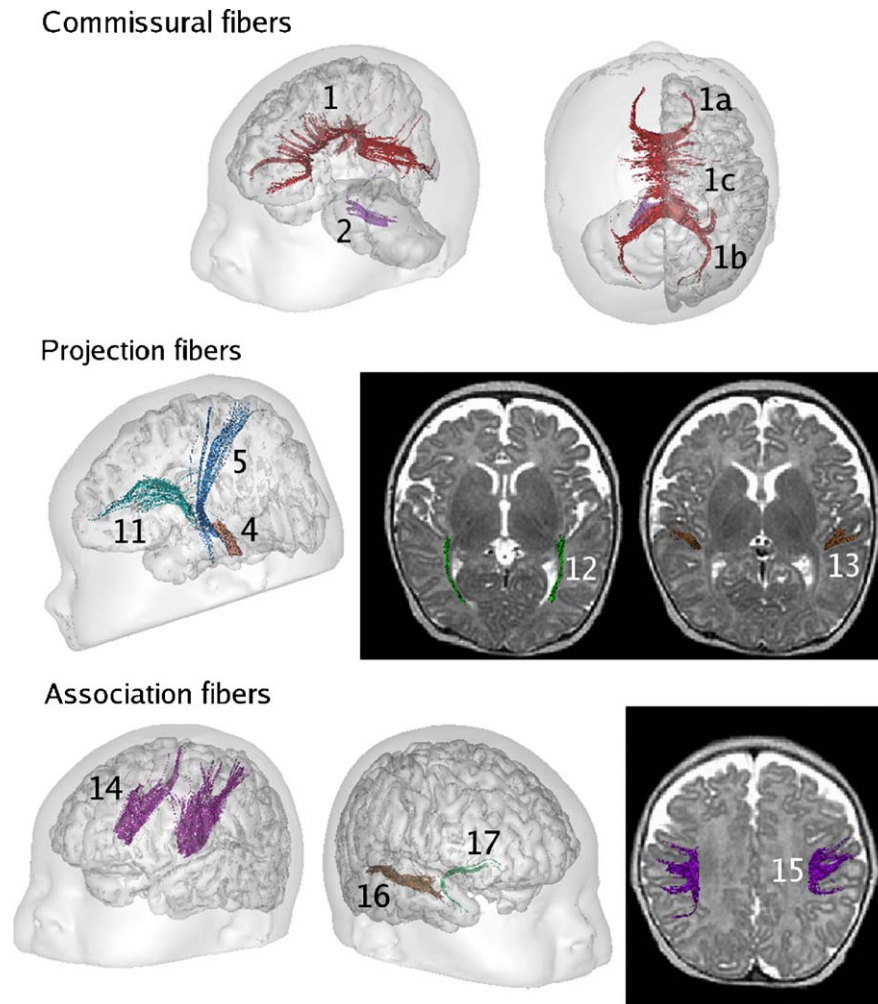


Fig. 3. Bundles tractography: tracked bundles in the brain of the same infant (see the text for the number significance), in 3D views (with the reconstructed infant's face and cortical surface), or 2D views (projection on anatomical images).

Quantification methods: ROIs vs. tracts

The results obtained with the two approaches were compared. However no validation could be performed due to a lack of reference in infants white matter bundles.

First, the analysis over split tracts led to significantly lower FA and higher $\langle D \rangle$ measurements compared with the analysis by ROIs for most of the bundles (Table 2, Fig. 6), probably because quantification was performed in a bigger VOI for tracts. No difference in FA was observed for the cortico-spinal tract (5), the optic radiations (12) and the external capsule (14). No difference in $\langle D \rangle$ was observed for the anterior limb of the internal capsule (11), the external capsule (14) and the uncinatus fasciculus (18). FA was statistically higher with the tract method for the cortico-spinal tract between the internal capsule and the low centrum semiovale (8); $\langle D \rangle$ was statistically lower for this latter segment (8), the whole tract (5) and the segment between the cerebral peduncles and the internal capsule (7). Besides, the same pattern of FA and $\langle D \rangle$ variations across bundles was observed with both methods; this pattern depends both on the differential bundles maturation and geometry (fibers compacity, crossing fibers).

Second, the two approaches were equivalent for the monitoring of the diffusion parameters changes with age, except for some bundles (Table 2). The tract analysis provided more relevant

information compared to the analysis over ROIs for the detection of the FA increase in the spino-thalamic tract, the posterior limb of the internal capsule, the optic radiations and the inferior longitudinal fasciculus. Actually, tracking was required to precisely locate and differentiate the optic radiations and the inferior longitudinal fasciculus because these fascicles merge in the occipital region; the ROI location in the bundles may have been variable across infants due to different bundles geometry.

Third, once corrected for significant evolution with age, the FA standard deviations in the bundles across infants were smaller with the tract approach than with the ROI approach (Table 2, Fig. 6) (two-tailed paired t test across bundles: $P = 0.000$). The standard deviations were not significantly different for $\langle D \rangle$.

Discussion

This study demonstrates the potential of DTI and tractography to assess the early 3D organization and the maturation of infants' white matter bundles. Despite unachieved myelination, main fiber bundles are already in place at birth, and they were mapped although FA was low. An original quantification approach, which considers the 3D tracked bundles, was used for monitoring the

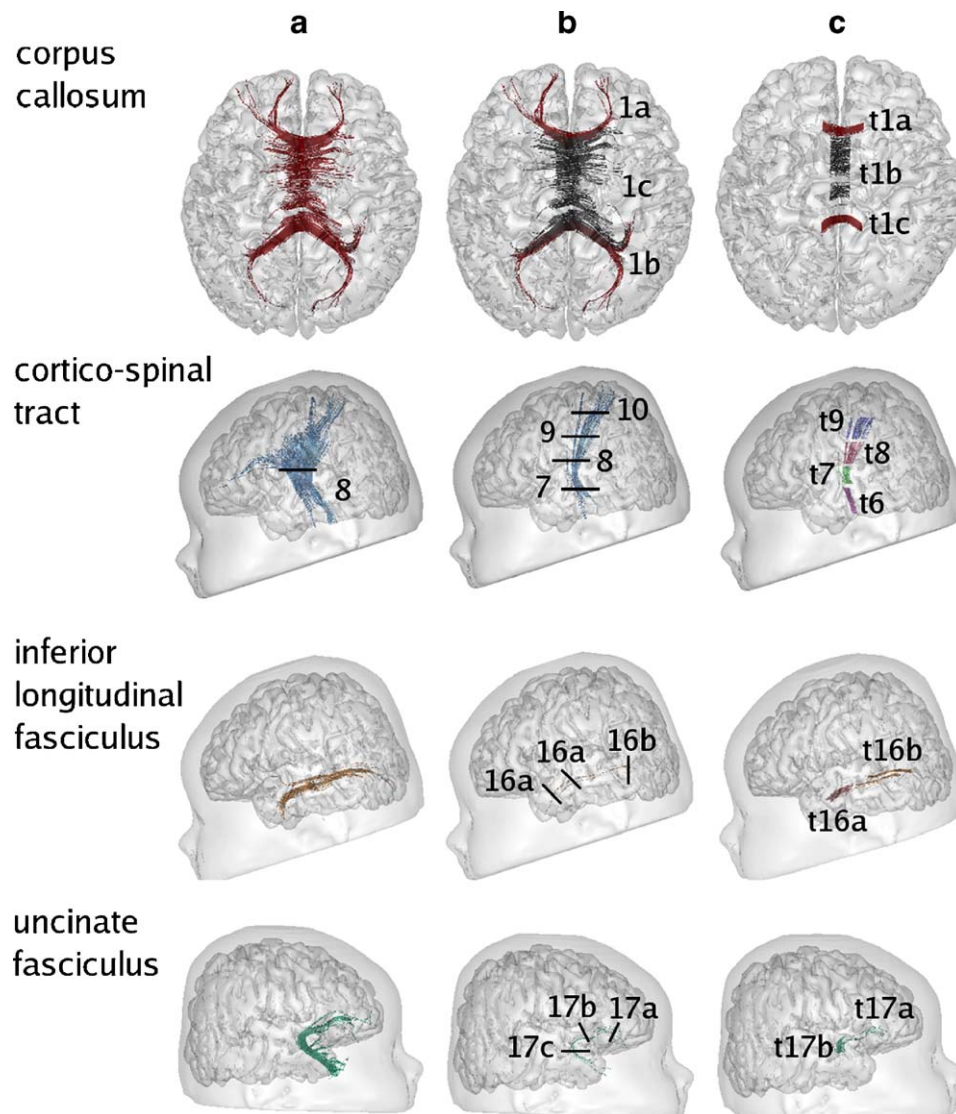


Fig. 4. Bundles reliability and splitting: tracked fibers, before (a) and after (b) constraints by “selection regions”, and split tracts considered for the quantitative analysis (c). Corpus callosum: b: classification in genu (1a), splenium (1b) and body (1c). Cortico-spinal tract: a: fibers tracked from a seed drawn in the posterior limb of the internal capsule (8); b: fibers passing through the cerebral peduncles (7) to the high centrum semiovale (10); c: split of the tract in four segments. Inferior longitudinal fasciculus: c: split of the tract in the temporal (t16a) and occipital (t16b) regions. Uncinate fasciculus: c: split of the tract in the frontal (t17a) and temporal (t17b) regions.

subtle evolution of the diffusion parameters with age, during a post-natal period critical for the infant psycho-motor development. This approach was compared to the conventional ROI approach.

First, a specific acquisition protocol, customized to the specific biological properties of the immature infant brain, was implemented. The mean diffusivity and the SNR are higher than in adults because of the higher water content and the longer T2 relaxation time (Neil et al., 1998; Mukherjee et al., 2002). A b factor of 700 s mm^{-2} was thus chosen to fit with the optimization described by Xing et al. (1997), and increasing the acquired number of orientations enabled to improve the accuracy of the diffusion tensor estimation (Bastin et al., 1998; Jones et al., 1999; Jones, 2004). The spatial resolution adjustment resulted from a compromise between the SNR and the acquisition time. Given the large voxel size compared to the small infant brain and the acquired number of orientations, partial volume effects in voxels containing crossing fibers could not be completely avoided. Nevertheless,

solving this common DTI pitfall would have required acquisition times not compatible with our unsedated pediatric population.

The major white matter bundles were tracked in the infants' brain despite low anisotropy, with a FA threshold of 0.1. A 0.2 threshold, which is generally considered in adults studies, was excluded because the tracking of the less mature tracts (like the uncinate fasciculus) was limited. As the “true” bundle size cannot be known, using large seeds and several selection regions significantly decreased the weight of any arbitrary choice of tracking parameters (Huang et al., 2004). The reliability of the fibers and of the “apparent” tract size was then increased. This method obviously implies that the fibers trajectory is known a priori and that inter-individual variability is reduced, which might not be the case for some bundles (e.g. the superior longitudinal fasciculus). Besides, the tracking accuracy may be affected by the background noise in the raw images, particularly for linear algorithms as errors accumulate with the line propagation (Basser

Table 2

FA (a) and $\langle D \rangle$ (b) results for all infants, evaluated for each bundle using both quantitative methods (averaged over ROIs or split tracts)

Bundle	Change per week of age (<i>P</i> value)		Mean \pm standard deviation		
	ROIs	Tracts	ROIs	Tracts	
(a) FA					
Corpus callosum:	1	0.011 (0.019)	0.006 (0.030)	0.56 \pm 0.05	0.45 \pm 0.03*
Genu	1a	(ns)	(ns)	0.64 \pm 0.07	0.52 \pm 0.05*
Splenium	1b	0.011 (0.012)	0.008 (0.018)	0.67 \pm 0.05	0.52 \pm 0.04*
Body	1c	0.013 (0.027)	0.006 (0.045)	0.46 \pm 0.07	0.34 \pm 0.03*
Mid cerebellar peduncles	2	(ns)	–	0.56 \pm 0.05	–
Pontine crossing tract	3	0.008 (0.04)	–	0.33 \pm 0.05	–
Spino-thalamic tract	4	(ns)	0.007 (0.018)	0.45 \pm 0.04	0.38 \pm 0.03*
Cortico-spinal tract:	5	0.006 (0.012)	0.006 (0.004)	0.47 \pm 0.02	0.48 \pm 0.02
In the midbrain	6–7	0.009 (0.007)	0.008 (0.006)	0.43 \pm 0.03	0.40 \pm 0.03*
Cerebral peduncles	7–8	0.010 (0.001)	0.010 (0.004)	0.55 \pm 0.03	0.53 \pm 0.03*
ic posterior limb	8–9	(ns)	0.007 (0.018)	0.51 \pm 0.03	0.57 \pm 0.03 ^o
Centrum semiovale	9–10	(ns)	(ns)	0.43 \pm 0.03	0.33 \pm 0.02*
ic anterior limb	11	0.006 (0.009)	0.004 (0.018)	0.43 \pm 0.03	0.34 \pm 0.02*
Optic radiations	12	(ns)	0.006 (0.008)	0.38 \pm 0.03	0.38 \pm 0.02
Acoustic radiations	13	0.008 (0.007)	–	0.28 \pm 0.03	–
External capsule	14	0.007 (0.009)	0.004 (0.023)	0.36 \pm 0.03	0.35 \pm 0.02
Superior longitudinal	15	0.005 (0.051)	–	0.36 \pm 0.03	–
Inferior longitudinal:	16	(ns)	0.004 (0.048)	0.38 \pm 0.03	0.32 \pm 0.02*
In the temporal region	16a	(ns)	(ns)	0.35 \pm 0.03	0.28 \pm 0.02*
In the occipital region	16b	(ns)	(ns)	0.41 \pm 0.04	0.36 \pm 0.03*
Uncinate:	17	(ns)	(ns)	0.36 \pm 0.03	0.31 \pm 0.02*
In the frontal region	17a	(ns)	(ns)	0.38 \pm 0.03	0.29 \pm 0.02*
In the temporal region	17b	(ns)	(ns)	0.36 \pm 0.03	0.33 \pm 0.03*
Cingulum	18	0.009 (0.009)	–	0.36 \pm 0.04	–
“All”	19	0.006 (0.000)	0.006 (0.004)	0.43 \pm 0.01	0.37 \pm 0.01*
(b) $\langle D \rangle (\times 10^{-3} \text{ mm}^2 \text{ s}^{-1})$					
Corpus callosum:	1	–0.023 (0.003)	–0.015 (0.017)	1.33 \pm 0.09	1.49 \pm 0.08*
Genu	1a	–0.021 (0.035)	(ns)	1.25 \pm 0.15	1.48 \pm 0.11*
Splenium	1b	–0.027 (0.000)	–0.016 (0.001)	1.22 \pm 0.07	1.39 \pm 0.05*
Body	1c	–0.022 (0.016)	–0.020 (0.028)	1.42 \pm 0.12	1.58 \pm 0.11*
Mid cerebellar peduncles	2	–0.011 (0.014)	–	0.96 \pm 0.05	–
Pontine crossing tract	3	–0.010 (0.004)	–	0.95 \pm 0.04	–
Spino-thalamic tract	4	(ns)	(ns)	0.92 \pm 0.04	1.00 \pm 0.06*
Cortico-spinal tract:	5	–0.010 (0.001)	–0.008 (0.005)	1.07 \pm 0.03	1.04 \pm 0.03 ^o
In the midbrain	6–7	–0.016 (0.000)	–0.019 (0.035)	1.11 \pm 0.04	1.19 \pm 0.12*
Cerebral peduncles	7–8	–0.016 (0.000)	–0.008 (0.005)	1.09 \pm 0.04	1.01 \pm 0.03 ^o
ic posterior limb	8–9	–0.006 (0.026)	–0.005 (0.036)	1.00 \pm 0.04	0.99 \pm 0.03 ^o
Centrum semiovale	9–10	–0.008 (0.019)	–0.009 (0.005)	1.10 \pm 0.04	1.14 \pm 0.04*
ic anterior limb	11	–0.009 (0.008)	–0.009 (0.005)	1.07 \pm 0.04	1.07 \pm 0.04
Optic radiations	12	–0.019 (0.002)	–0.032 (0.000)	1.25 \pm 0.07	1.31 \pm 0.07*
Acoustic radiations	13	–0.015 (0.013)	–	1.14 \pm 0.07	–
External capsule	14	–0.014 (0.001)	–0.010 (0.000)	1.07 \pm 0.04	1.09 \pm 0.03
Superior longitudinal	15	–0.015 (0.005)	–	1.18 \pm 0.06	–
Inferior longitudinal:	16	–0.016 (0.000)	–0.019 (0.001)	1.24 \pm 0.04	1.34 \pm 0.05*
In the temporal region	16a	–0.011 (0.004)	–0.014 (0.005)	1.27 \pm 0.04	1.33 \pm 0.05*
In the occipital region	16b	–0.020 (0.000)	–0.022 (0.000)	1.21 \pm 0.05	1.34 \pm 0.06*
Uncinate:	17	–0.013 (0.000)	–0.010 (0.001)	1.16 \pm 0.02	1.18 \pm 0.03
In the frontal region	17a	–0.015 (0.000)	–0.012 (0.000)	1.18 \pm 0.04	1.22 \pm 0.03*
In the temporal region	17b	–0.011 (0.000)	–0.009 (0.003)	1.12 \pm 0.03	1.15 \pm 0.03*
Cingulum	18	–0.014 (0.002)	–	1.19 \pm 0.05	–
“All”	19	–0.014 (0.000)	–0.014 (0.000)	1.14 \pm 0.02	1.19 \pm 0.02*

In the two central columns, changes with age, corrected by gestational age at birth, are detailed for statistically significant linear correlations (in parenthesis: *P* values, ns: not significant). In the two right columns, the mean values and standard deviations over infants are presented, and significant differences between methods are outlined: *: lower FA and higher $\langle D \rangle$ with the tract approach; ^o: higher FA and lower $\langle D \rangle$ with the tract approach.

For an easier comparison of the ROI and tract quantification, parameters for adjacent ROIs of the cortico-spinal tract and the uncinate fasciculus have been averaged (so that equivalent regions are considered for ROIs and tracts).

* Lower FA and higher $\langle D \rangle$ with the tract approach.

^o Higher FA and lower $\langle D \rangle$ with the tract approach.

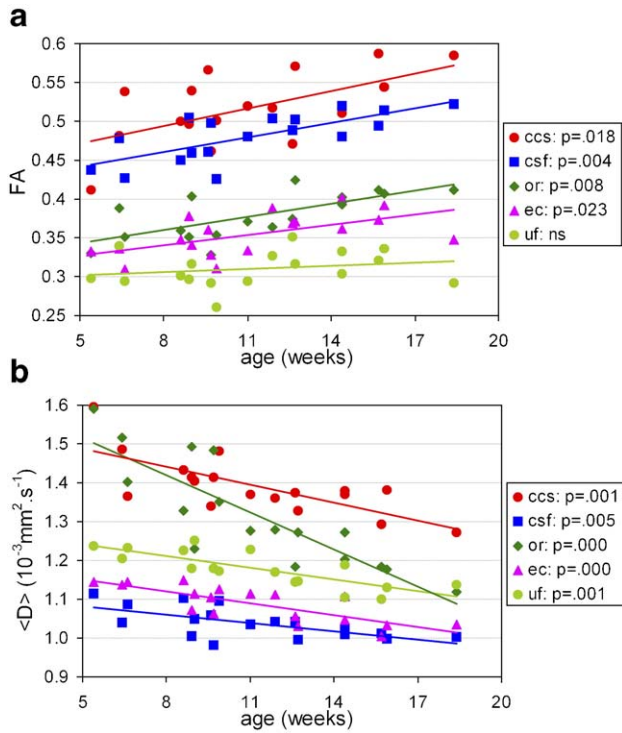


Fig. 5. Diffusion parameters evolution with age: FA (a) and $\langle D \rangle$ (b) changes with infants' age, corrected by gestational age at birth, for examples of bundles (from Table 2): ccs: corpus callosum splenium; csf: cortico-spinal fibers; or: optic radiations; ec: external capsule; uf: uncinate fasciculus. FA and $\langle D \rangle$ were quantified on average over sections of the tracts. Significant P values are outlined (ns: not significant).

et al., 2000; Lazar and Alexander, 2003). Therefore we attempted to acquire images with high and reproducible SNR among infants. Under this restrictive methodology, anatomically plausible tracts were obtained.

References on the white matter bundles organization are lacking in infants. In our study, this organization appeared very similar to adults (Wakana et al., 2004). Nevertheless, our method still presents limitations. Some bundles, although present, might have not been tracked, because of the spatial resolution or the low anisotropy resulting from the low myelination. As crossing fibers are not handled properly with the diffusion tensor concept, erroneous fibers may be tracked, and, if a bundle is visible in infants and not in adults, one may speculate whether this connection may disappear with maturation or whether it is an artefact. Non-linear tractography algorithms would be interesting to consider, such as methods based on probabilistic approaches (Hagmann et al., 2003; Parker et al., 2003; Lazar and Alexander, 2005), or on the minimization of the fibers global energy, with regularization of their trajectory (Poupon et al., 2000). Another obvious limitation of the tracking method is that the distinction between afferent and efferent fibers cannot be made with diffusion MRI by principles.

So far, DTI has been used to describe and quantify the white matter maturation and myelination processes in preterm or at term newborns (Neil et al., 1998; Huppi et al., 1998a, 2001; Miller et al., 2002; Zhai et al., 2003; Partridge et al., 2004; Gilmore et al., 2004), and in children over a large range of ages, from birth through childhood or adolescence (Klingberg et al., 1999; Mukherjee et al., 2002; McGraw et al., 2002; Boujraf et al., 2002; Schmithorst et al.,

2002; Schneider et al., 2004; Hermoye et al., in press). The study of healthy infants from 1 to 4 months old has not been reported yet. We focused on this critical period as major changes occur during the first months of life: cerebral growth and maturation (synaptogenesis, myelination) are intense while the brain encounters numerous external stimulations after birth. Imaging this subject population was challenging and required patience because we did not sedate healthy infants for ethical reasons. Reliable data were obtained only for 70% of the subjects. A large group of 18 infants was studied in order to assess the reliability and reproducibility of the proposed approach.

A reliable method for defining VOIs for the diffusion parameters quantification was required in order to monitor the subtle changes happening during this developmental period across bundles. The tracking approach, which was initially described for the evaluation of the pyramidal tract of infants and children with congenital hemiparesis (Glenn et al., 2003), was compared to an approach with polygonal ROIs, which were described to generate more reliable results than elliptical ROIs (Bonekamp et al., 2005). The results reproducibility was assessed by two different means. The feasibility of following changes with age in most bundles was the first warrant: if the bundles were not precisely localized across infants, no effects would have been observed. Second, the standard deviations across infants, once corrected for evolution with age, were small. From a methodological point of view (Partridge et al., 2005), the tracking approach should be preferred, except for

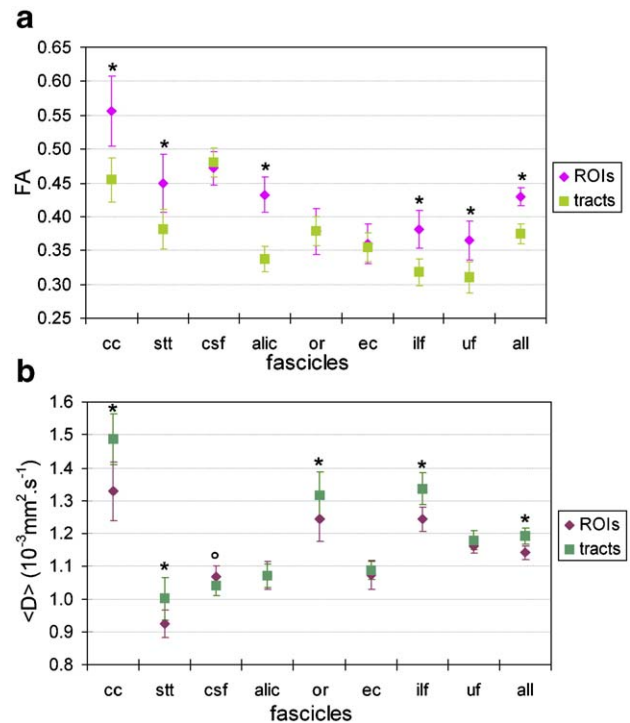


Fig. 6. Diffusion parameters averages over infants: FA (a) and $\langle D \rangle$ (b) mean values and standard deviations (error bars) over infants: evaluated with the two quantitative methods (averages over ROIs or split tracts), for examples of bundles (from Table 2): cc: corpus callosum; stt: spino-thalamic tract; csf: cortico-spinal fibers; alic: anterior limb of the internal capsule; or: optic radiations; ec: external capsule; ilf: inferior longitudinal fasciculus; uf: uncinate fasciculus; all: average over tracts. Statistically significant differences between methods are outlined: *: lower FA and higher $\langle D \rangle$ with the tract approach; °: higher FA and lower $\langle D \rangle$ with the tract approach

bundles (like the cingulum or the acoustic radiations) which cannot be reproducibly delimited across subjects. Actually, the ROI approach is open to bias because the location reproducibility across subjects depends on the experimenter expertise. The bundles are better delineated with the tracking method, in an easier way, and partial volume effects are reduced. Furthermore, the bundle is considered as a whole and the analysis is not focused on a reduced region. In this study, both methods led to similar results concerning the differential maturation process of the bundles. However, absolute FA and $\langle D \rangle$ values were different for some bundles, which may essentially result from a difference in the VOIs size (the ROIs had to be small to ensure a localization within the bundles core, whereas the whole bundle was tracked). None quantification could be validated due to a lack of reference in infants white matter bundles. Furthermore, the comparison of FA standard deviations over infants with both approaches confirmed that the latter one should be preferred. On the other hand, since the maturation differs along the bundle, with myelination progressing in the direction of the impulse conduction (Van der Knaap and Valk, 1995), the method which consists of averaging the diffusion parameters over the whole tract may also be questionable. The more accurate way to evaluate the fasciculus maturation would be to consider the diffusion parameters along the tract (Gong et al., 2005; Berman et al., in press), but it would be difficult to systematically assess the evolution with age for all bundles.

Both FA and $\langle D \rangle$ changes with age were monitored in order to describe the bundles maturation. FA was described to be the most sensitive marker for detecting differences between tracts in the premature brain (Partridge et al., 2004). In our study, both parameters provided relevant and complementary informations. The observation of FA and / or $\langle D \rangle$ variations might depend on partial volume effects: when spatial resolution is critical (like for the uncinat fasciculus), a change in $\langle D \rangle$, but not in FA, might be obtained. On the other hand, these variations might rely on the maturation stages of the bundles. The decrease in $\langle D \rangle$ might highlight the decrease in water content resulting from the axonal maturation (with membranes, organelles and microtubules maturation), the increase in fibers density and the first stage of oligodendroglial proliferation, whereas the increase in FA might rather reflect changes which accompany the “premyelinating state”, the last stage of “true” myelination with wrapping of the myelin sheath around the axons and the increasing organization and compacity of the bundles (Neil et al., 2002). The FA increase with age may hardly result from larger partial volume effects between gray and white matters in the younger infants, as the ROIs and split tracts locations in the white matter were visually checked on the $b = 0$ image. Segmentation of the unmyelinated infant brain tissues could not be achieved because it requires the acquisition of complementary conventional images (as the contrast in T1 is low, Huppi et al., 1998b), which was precluded for unsedated infants.

Furthermore, the infants maturational age, i.e. corrected by gestational age at birth, was here considered because the infants gestational term ranged from 37 to 41 weeks. The fact that brain maturation differs before and after birth was not taken into account. This should be investigated through the comparison of diffusion parameters changes with ages corrected or not by the gestational age: the respective roles of intra-uterine growth and post-natal environment on brain development and white matter maturation might then be better understood.

The differential changes with age observed across bundles are in good agreement with the known stages of myelination, as

studied in postmortem studies. Myelination is known to begin earlier in the commissural and projection fibers than in the association fibers, and earlier in the occipital and temporal lobes than in the frontal lobe (Yakovlev and Lecours, 1967; Brody et al., 1987). However, the origins of water diffusion anisotropy in DTI are still debated (for review Beaulieu, 2002) since it exists in “premyelinating states” (Wimberger et al., 1995; Huppi et al., 1998a; Prayer et al., 2001) or in non-myelinated nerves (Beaulieu and Allen, 1994; Ono et al., 1995; Gulani et al., 2001; Song et al., 2002). Increase in FA with age may not only rely on myelination but may also result in an increase in the fibers density and in the bundles volume.

Finally, a non-invasive classification of the differential bundles maturation may be provided using the proposed approach by comparing the infant population to an adult population in order to normalize for differences in bundles geometry and compactness.

Conclusion

DTI combined with fiber tracking appears as a promising tool for highlighting the early organization and maturation of white matter bundles in young infants, as well as pathological (absent or delayed) white matter development, like in premature newborns or after a perinatal stroke. Compared with functional tests (like functional MRI), the link between structural and functional developments should be better understood.

Acknowledgments

The authors thank Stéren Chabert and Carlos Meca for discussion on the diffusion phenomenon, Franck Lethimonnier, Cyril Poupon, Denis Rivière, Edouard Duchesnay and Arnaud Cachia for support on the DTI acquisition and the post-processings, Jean-François Mangin for infant brains 3D rendering, Mr. Brunet from Ravier-Touzard Company for designing a baby bouncer chair specifically adapted to the head coil and the McDonnell foundation for financial support.

References

- Baratti, C., Barnett, A.S., Pierpaoli, C., 1999. Comparative MR imaging study of brain maturation in kittens with T1, T2, and the trace of the diffusion tensor. *Radiology* 210, 133–142.
- Barkovich, A.J., Kjos, B.O., Jackson Jr., D.E., Norman, D., 1988. Normal maturation of the neonatal and infant brain: MR imaging at 1.5 T. *Radiology* 166, 173–180.
- Basser, P.J., Jones, D.K., 2002. Diffusion-tensor MRI: theory, experimental design and data analysis—A technical review. *NMR Biomed.* 15, 456–467.
- Basser, P.J., Pierpaoli, C., 1996. Microstructural and physiological features of tissues elucidated by quantitative-diffusion-tensor MRI. *J. Magn. Reson., B* 111, 209–219.
- Basser, P.J., Mattiello, J., LeBihan, D., 1994. MR diffusion tensor spectroscopy and imaging. *Biophys. J.* 66, 259–267.
- Basser, P.J., Pajevic, S., Pierpaoli, C., Duda, J., Aldroubi, A., 2000. In vivo fiber tractography using DT-MRI data. *Magn. Reson. Med.* 44, 625–632.
- Bastin, M.E., Armitage, P.A., Marshall, I., 1998. A theoretical study of the effect of experimental noise on the measurement of anisotropy in diffusion imaging. *Magn. Reson. Imaging* 16, 773–785.

- Beaulieu, C., 2002. The basis of anisotropic water diffusion in the nervous system—A technical review. *NMR Biomed.* 15, 435–455.
- Beaulieu, C., Allen, P.S., 1994. Determinants of anisotropic water diffusion in nerves. *Magn. Reson. Med.* 31, 394–400.
- Berman, J.I., Mukherjee, P., Partridge, S.C., Miller, S.P., Ferriero, D.M., Barkovich, A.J., Vigneron, D.B., Henry, R.G., in press. Quantitative diffusion tensor MRI fiber tractography of sensorimotor white matter development in premature infants. *Neuroimage*.
- Bonekamp, D., Nagae-Poetscher, L.M., Degaonkar, M., Matson, M., Mori, S., Horska, A., 2005. Intra-rater and inter-rater reproducibility of FA and ADC: a clinical pediatric DTI study. Proceedings of the 13th ISMRM Scientific Meeting, Miami, Florida, #648.
- Boujraf, S., Luybaert, R., Shabana, W., De Meirleir, L., Sourbron, S., Osteaux, M., 2002. Study of pediatric brain development using magnetic resonance imaging of anisotropic diffusion. *Magn. Reson. Imaging* 20, 327–336.
- Brody, B.A., Kinney, H.C., Kroman, A.S., Gilles, F.H., 1987. Sequence of central nervous system myelination in human infancy: I. An autopsy study of myelination. *J. Neuropathol. Exp. Neurol.* 46, 283–301.
- Catani, M., Howard, R.J., Pajevic, S., Jones, D.K., 2002. Virtual in vivo interactive dissection of white matter fasciculi in the human brain. *NeuroImage* 17, 77–94.
- Catani, M., Jones, D.K., Donato, R., Ffytche, D.H., 2003. Occipito-temporal connections in the human brain. *Brain* 126, 2093–2107.
- Cointepas, Y., Mangin, J.F., Garnero, L., Poline, J.B., Benali, H., 2001. BrainVISA: Software platform for visualization and analysis of multi-modality brain data. Proceedings of the 7th HBM Scientific Meeting, Brighton, United Kingdom, *NeuroImage*, p. S98.
- Cointepas, Y., Poupon, C., Maroy, R., Riviere, D., Le Bihan, D., Mangin, J.F., 2003. A freely available Anatomist/BrainVISA package for analysis of diffusion MR data. Proceedings of the 9th HBM Scientific Meeting, New York, USA, *NeuroImage* 19, p. S810.
- Conturo, T.E., Lori, N.F., Cull, T.S., Akbudak, E., Snyder, A.Z., Shimony, J.S., McKinstry, R.C., Burton, H., Raichle, M.E., 1999. Tracking neuronal fiber pathways in the living human brain. *Proc. Natl. Acad. Sci.* 96, 10422–10427.
- Dubois, J., Poupon, C., Cointepas, Y., Lethimonnier, F., Le Bihan, D., 2004. Diffusion gradient orientation schemes for DTI acquisitions with quiet subjects. Proceedings of the 12th ISMRM Scientific Meeting, Kyoto, Japan, #443.
- Gilmore, J.H., Zhai, G., Wilber, K., Smith, J.K., Lin, W., Gerig, G., 2004. 3 Tesla magnetic resonance imaging of the brain in newborns. *Psychiatry Res.* 132, 81–85.
- Glenn, O.A., Henry, R.G., Berman, J.I., Chang, P.C., Miller, S.P., Vigneron, D.B., Barkovich, A.J., 2003. DTI-based three-dimensional tractography detects differences in the pyramidal tracts of infants and children with congenital hemiparesis. *J. Magn. Reson. Imaging* 18, 641–648.
- Gong, G., Jiang, T., Zhu, C., Zang, Y., Wang, F., Xie, S., Xiao, J., Guo, X., 2005. Asymmetry analysis of cingulum based on scale-invariant parameterization by diffusion tensor imaging. *Hum. Brain Mapp.* 24, 92–98.
- Gulani, V., Webb, A.G., Duncan, I.D., Lauterbur, P.C., 2001. Apparent diffusion tensor measurements in myelin-deficient rat spinal cords. *Magn. Reson. Med.* 45, 191–195.
- Hagmann, P., Thiran, J.P., Jonasson, L., Vandergheynst, P., Clarke, S., Maeder, P., Meuli, R., 2003. DTI mapping of human brain connectivity: statistical fiber tracking and virtual dissection. *NeuroImage* 19, 545–554.
- Hermoye, L., Saint-Martin, C., Cosnard, G., Lee, S.K., Kim, J., Nassogne, M.C., Menten, R., Clapuyt, P., Donohue, P.K., Hua, K., Wakana, S., Jiang, H., van Zijl, P.C., in press. Mori S. Pediatric diffusion tensor imaging: Normal database and observation of the white matter maturation in early childhood. *Neuroimage*.
- Huang, H., Zhang, J., van Zijl, P.C., Mori, S., 2004. Analysis of noise effects on DTI-based tractography using the brute-force and multi-ROI approach. *Magn. Reson. Med.* 52, 559–565.
- Huppi, P.S., Maier, S.E., Peled, S., Zientara, G.P., Barnes, P.D., Jolesz, F.A., Volpe, J.J., 1998a. Microstructural development of human newborn cerebral white matter assessed in vivo by diffusion tensor magnetic resonance imaging. *Pediatr Res.* 44, 584–590.
- Huppi, P.S., Warfield, S., Kikinis, R., Barnes, P.D., Zientara, G.P., Jolesz, F.A., Tsudi, M.K., Volpe, J.J., 1998b. Quantitative magnetic resonance imaging of brain development in premature and mature newborns. *Ann. Neurol.* 43, 224–235.
- Huppi, P.S., Murphy, B., Maier, S.E., Zientara, G.P., Inder, T.E., Barnes, P.D., Kikinis, R., Jolesz, F.A., Volpe, J.J., 2001. Microstructural brain development after perinatal cerebral white matter injury assessed by diffusion tensor magnetic resonance imaging. *Pediatrics* 107, 455–460.
- Jones, D.K., 2004. The effect of gradient sampling schemes on measures derived from diffusion tensor MRI: A Monte Carlo study. *Magn. Reson. Med.* 51, 807–815.
- Jones, D.K., Horsfield, M.A., Simmons, A., 1999. Optimal strategies for measuring diffusion in anisotropic systems by magnetic resonance imaging. *Magn. Reson. Med.* 42, 515–525.
- Klingberg, T., Vaidya, C.J., Gabrieli, J.D., Moseley, M.E., Hedehus, M., 1999. Myelination and organization of the frontal white matter in children: a diffusion tensor MRI study. *NeuroReport* 10, 2817–2821.
- Lazar, M., Alexander, A.L., 2003. An error analysis of white matter tractography methods: synthetic diffusion tensor field simulations. *NeuroImage* 20, 1140–1153.
- Lazar, M., Alexander, A.L., 2005. Bootstrap white matter tractography (BOOT-TRAC). *NeuroImage* 24, 524–532.
- Le Bihan, D., 2003. Looking into the functional architecture of the brain with diffusion MRI. *Nat. Rev., Neurosci.* 4, 469–480.
- Le Bihan, D., Breton, E., Lallemand, D., Grenier, P., Cabanis, E., Laval-Jeantet, M., 1986. MR imaging of intravoxel incoherent motions: application to diffusion and perfusion in neurologic disorders. *Radiology* 161, 401–407.
- Le Bihan, D., Mangin, J.F., Poupon, C., Clark, C.A., Pappata, S., Molko, N., Chabriat, H., 2001. Diffusion tensor imaging: concepts and applications. *J. Magn. Reson. Imaging* 13, 534–546.
- Mangin, J.F., Poupon, C., Clark, C., Le Bihan, D., Bloch, I., 2002. Distortion correction and robust tensor estimation for MR diffusion imaging. *Med. Image Anal.* 6, 191–198.
- McGraw, P., Liang, L., Provenzale, J.M., 2002. Evaluation of normal age-related changes in anisotropy during infancy and childhood as shown by diffusion tensor imaging. *Am. J. Roentgenol.* 179, 1515–1522.
- Miller, S.P., Vigneron, D.B., Henry, R.G., Bohland, M.A., Ceppi-Cozzio, C., Hoffman, C., Newton, N., Partridge, J.C., Ferriero, D.M., Barkovich, A.J., 2002. Serial quantitative diffusion tensor MRI of the premature brain: Development in newborns with and without injury. *J. Magn. Reson. Imaging* 16, 621–632.
- Mori, S., van Zijl, P.C., 2002. Fiber tracking: principles and strategies—A technical review. *NMR Biomed.* 15, 468–480.
- Mori, S., Crain, B.J., Chacko, V.P., van Zijl, P.C., 1999. Three-dimensional tracking of axonal projections in the brain by magnetic resonance imaging. *Ann. Neurol.* 45, 265–269.
- Mori, S., Kaufmann, W.E., Davatzikos, C., Stieltjes, B., Amodei, L., Fredericksen, K., Pearlson, G.D., Melhem, E.R., Solaiyappan, M., Raymond, G.V., Moser, H.W., van Zijl, P.C., 2002. Imaging cortical association tracts in the human brain using diffusion-tensor-based axonal tracking. *Magn. Reson. Med.* 47, 215–223.
- Moseley, M.E., Cohen, Y., Kucharczyk, J., Mintorovitch, J., Asgari, H.S., Wendland, M.F., Tsuruda, J., Norman, D., 1990. Diffusion-weighted MR imaging of anisotropic water diffusion in cat central nervous system. *Radiology* 176, 439–445.
- Mukherjee, P., Miller, J.H., Shimony, J.S., Conturo, T.E., Lee, B.C., Almlí, C.R., McKinstry, R.C., 2001. Normal brain maturation during childhood: developmental trends characterized with diffusion-tensor MR imaging. *Radiology* 221, 349–358.
- Mukherjee, P., Miller, J.H., Shimony, J.S., Philip, J.V., Nehra, D., Snyder, A.Z., Conturo, T.E., Neil, J.J., McKinstry, R.C., 2002. Diffusion-Tensor MR Imaging of gray and white matter development during normal human brain maturation. *Am. J. Neuroradiol.* 23, 1445–1456.
- Neil, J.J., Shiran, S.I., McKinstry, R.C., Scheff, G.L., Snyder, A.Z., Almlí,

- C.F., Akbudak, E., Aronovitz, J.A., Miller, J.P., Lee, B.C., Conturo, T.E., 1998. Normal brain in human newborns: apparent diffusion coefficient and diffusion anisotropy measured by using diffusion tensor MR imaging. *Radiology* 15, 57–66.
- Neil, J.J., Miller, J., Mukherjee, P., Huppi, P.S., 2002. Diffusion tensor imaging of normal and injured developing human brain—A technical review. *NMR Biomed.* 15, 543–552.
- Ono, J., Harada, K., Takahashi, M., Maeda, M., Ikenaka, K., Sakurai, K., Sakai, N., Kagawa, T., Fritz-Zieroth, B., Nagai, T., et al., 1995. Differentiation between dysmyelination and demyelination using magnetic resonance diffusional anisotropy. *Brain Res.* 671, 141–148.
- Pajevic, S., Pierpaoli, C., 1999. Color schemes to represent the orientation of anisotropic tissues from diffusion tensor data: application to white matter fiber tract mapping in the human brain. *Magn. Reson. Med.* 42, 526–540.
- Parker, G.J., Haroon, H.A., Wheeler-Kingshott, C.A., 2003. A framework for a streamline-based probabilistic index of connectivity (PICO) using a structural interpretation of MRI diffusion measurements. *J. Magn. Reson. Imaging* 18, 242–254.
- Partridge, S.C., Mukherjee, P., Henry, R.G., Miller, S.P., Berman, J.I., Jin, H., Lu, Y., Glenn, O.A., Ferriero, D.M., Barkovich, A.J., Vigneron, D.B., 2004. Diffusion tensor imaging: serial quantitation of white matter tract maturity in premature newborns. *NeuroImage* 22, 1302–1314.
- Partridge, S.C., Mukherjee, P., Berman, J.I., Henry, R.G., Miller, S.P., Lu, Y., Glenn, O.A., Ferriero, D.M., Barkovich, A.J., Vigneron, D.B., 2005. Tractography-based quantitation of diffusion tensor imaging parameters in white matter tracts of preterm newborns. *J. Magn. Reson. Imaging* 22, 467–474.
- Paus, T., Collins, D.L., Evans, A.C., Leonard, G., Pike, B., Zijdenbos, A., 2001. Maturation of white matter in the human brain: a review of magnetic resonance studies. *Brain Res. Bull.* 54, 255–266.
- Pierpaoli, C., Basser, P.J., 1996. Toward a quantitative assessment of diffusion anisotropy. *Magn. Reson. Med.* 36, 893–906.
- Poupon, C., Clark, C.A., Frouin, V., Regis, J., Bloch, I., Le Bihan, D., Mangin, J., 2000. Regularization of diffusion-based direction maps for the tracking of brain white matter fascicles. *NeuroImage* 12, 184–195.
- Prayer, D., Barkovich, A.J., Kirschner, D.A., Prayer, L.M., Roberts, T.P., Kucharczyk, J., Moseley, M.E., 2001. Visualization of nonstructural changes in early white matter development on diffusion-weighted MR images: evidence supporting premyelination anisotropy. *Am. J. Neuro-radiol.* 22, 1572–1576.
- Riviere, D., Papadopoulos-Orfanos, D., Poupon, C., Poupon, F., Coulon, O., Poline, J.B., Frouin, V., Regis, J., Mangin, J.F., 2000. A structural browser for human brain mapping. *Proceedings of the 6th HBM Scientific Meeting, San Antonio, USA, NeuroImage* vol. 11, p. S912.
- Rutherford, M.A., Cowan, F.M., Manzur, A.Y., Dubowitz, L.M., Pennock, J.M., Hajnal, J.V., Young, I.R., Bydder, G.M., 1991. MR imaging of anisotropically restricted diffusion in the brain of neonates and infants. *J. Comput. Assist. Tomogr.* 15, 188–198.
- Sakuma, H., Nomura, Y., Takeda, K., Tagami, T., Nakagawa, T., Tamagawa, Y., Ishii, Y., Tsukamoto, T., 1991. Adult and neonatal human brain: diffusional anisotropy and myelination with diffusion-weighted MR imaging. *Radiology* 180, 229–233.
- Salamon, G., Raynaud, C., Regis, J., Rumeau, C., 1990. *Magnetic Resonance Imaging of the Pediatric Brain, An Anatomical Atlas*. Raven Press, New York.
- Schmithorst, V.J., Wilke, M., Dardzinski, B.J., Holland, S.K., 2002. Correlation of white matter diffusivity and anisotropy with age during childhood and adolescence: a cross-sectional diffusion-tensor MR imaging study. *Radiology* 222, 212–218.
- Schneider, J.F., Il'yasov, K.A., Hennig, J., Martin, E., 2004. Fast quantitative diffusion-tensor imaging of cerebral white matter from the neonatal period to adolescence. *Neuroradiology* 46, 258–266.
- Song, S.K., Sun, S.W., Ramsbottom, M.J., Chang, C., Russell, J., Cross, A.H., 2002. Dysmyelination revealed through MRI as increased radial (but unchanged axial) diffusion of water. *NeuroImage* 17, 1429–1436.
- Van der Knaap, M.S., Valk, J., 1990. MR imaging of the various stages of normal myelination during the first year of life. *Neuroradiology* 31, 459–470.
- Van der Knaap, M.S., Valk, J., 1995. Myelin and white matter. In: Van der Knaap, M.S., Valk, J. (Eds.), *Magnetic Resonance of Myelin, Myelination and Myelin Disorders*. Springer-Verlag, Berlin, pp. 1–17.
- Wakana, S., Jiang, H., Nagae-Poetscher, L.M., Zijl, P.C., Mori, S., 2004. *Fiber tract-based atlas of human white matter anatomy*. *Radiology* 230, 77–87.
- Wimberger, D.M., Roberts, T.P., Barkovich, A.J., Prayer, L.M., Moseley, M.E., Kucharczyk, J., 1995. Identification of “premyelination” by diffusion-weighted MRI. *J. Comput. Assist. Tomogr.* 19, 28–33.
- Xing, D., Papadakis, N.G., Huang, C.L., Lee, V.M., Carpenter, T.A., Hall, L.D., 1997. Optimised diffusion-weighting for measurement of apparent diffusion coefficient ($<D>$) in human brain. *Magn. Reson. Imaging* 15, 771–784.
- Yakovlev, P.I., Lecours, A.R., 1967. The myelogenetic cycles of regional maturation in the brain. In: Minowski A. (Ed.), *Regional Development of the Brain in Early Life*. Blackwell, Oxford, pp. 3–69.
- Yoo, S.S., Park, H.J., Soul, J.S., Mamata, H., Park, H., Westin, C.F., Bassan, H., Du Plessis, A.J., Robertson Jr., R.L., Maier, S.E., Ringer, S.A., Volpe, J.J., Zientara, G.P., 2005. In vivo visualization of white matter fiber tracts of preterm- and term-infant brains with diffusion tensor magnetic resonance imaging. *Invest. Radiol.* 40, 110–115.
- Zhai, G., Lin, W., Wilber, K.P., Gerig, G., Gilmore, J.H., 2003. Comparisons of regional white matter diffusion in healthy neonates and adults performed with a 3.0-T head-only MR imaging unit. *Radiology* 229, 673–681.